

# Effect of Co on microstructural stability of the third generation Ni-based single crystal superalloys

Bo Wang, Jun Zhang,<sup>a)</sup> Taiwen Huang, Wenchao Yang, Haijun Su, Zhuoran Li, Lin Liu, and Hengzhi Fu

*State Key Laboratory of Solidification Processing, Northwestern Polytechnical University, Xi'an 710072, China*

(Received 5 January 2016; accepted 25 February 2016)

The effect of Co on element segregation and microstructure is investigated in the third generation Ni-based single crystal superalloys with 4, 8.5, and 11.5 wt% Co addition. The results show that the increase of Co content leads to a severe element segregation in as-cast microstructure. After heat treatment, the size of  $\gamma'$  phase is slightly reduced with Co content increase. During the thermal exposure, the  $\gamma'$  phase coarsens gradually but its coarsening rate decreases with increasing Co content. In addition, some acicular and blocky topologically close-packed (TCP) phases are precipitated in 4% Co and 8.5% Co alloys. However, no TCP phase can be found in 11.5% Co alloy. Finally, it may be concluded that although a higher Co content is harmful for the element segregation, it is beneficial to maintain the cuboidal morphology of  $\gamma'$  phase, decrease its coarsening rate, and impede the precipitation of TCP phase.

## I. INTRODUCTION

Ni-based single crystal superalloys are widely used in the manufacture of aero engines turbine blades because of their superior high-temperature capability and good high temperature performance.<sup>1–3</sup> In the 1980s, the first generation single crystal superalloys were produced by the directional solidification technology. Currently, the commercial single crystal superalloys have been progressed to the fifth generation. The first three generation alloys contain 0% Re, 3% Re, and 6% Re, respectively. Afterward, 3% Ru and 6% Ru are introduced into the third generation superalloys to form the fourth and the fifth generation alloys to further increase the temperature capability with approximately 30 °C step.<sup>4–8</sup>

Microstructural stability during thermal exposure plays a very important role in controlling the mechanical property of Ni-based single crystal superalloys, which includes the precipitation of topologically close-packed (TCP) phase and the stability of  $\gamma'$  phase. In the third generation superalloys, the total amount of refractory elements reaches up to 20%. Therefore, they are prone to enrich in the local area of  $\gamma$  matrix, resulting in the precipitation of TCP phase and further decreasing in the high temperature performance.<sup>9–15</sup> For example, although the amounts of refractory elements were 20 and 19.4% in René N6 and CMSX-10 as the typical third single crystal superalloys, respectively, they presented a different precipitated tendency of TCP phase. The biggest difference

in alloy compositions was that they contained 12% and 3% Co contents, respectively. Therefore, there are lots of controversies about the effect of Co on the microstructural stability for a long time. Although Walston believed that high Co content could improve the microstructural stability,<sup>12,16</sup> Erickson believed that low Co content could reduce the precipitated tendency of TCP phase,<sup>17,18</sup> and Rae and Reed believed that the alloy with high Co content exhibited an excellent short-term stability and it was easy to form some coarse  $\mu$  phases after long-term thermal exposure.<sup>9</sup> Overall, the mechanism of Co element on TCP phase precipitation is still unclear.

In addition, the composition difference between  $\gamma$  and  $\gamma'$  phases resulting from the addition of Co content also inevitably affects the stability of the  $\gamma'$  phase. In other words, the composition difference of  $\gamma$  and  $\gamma'$  phases causes the change of elemental partitioning ratio to further modify the  $\gamma/\gamma'$  lattice misfit, which determines the morphology and stability of  $\gamma'$  phase.<sup>16,19–21</sup> Therefore, this paper reports on the effects of Co on the element segregation,  $\gamma'$  phase stability, and TCP phase precipitation of three Ni-based single crystal superalloys with different Co addition to accelerate the development of the new promising superalloy with improved microstructural stability and enhanced future alloy composition optimization.

## II. EXPERIMENTAL PROCEDURE

Three single crystal superalloys with 4 wt% Co, 8.5% Co, and 11.5% Co additions were designed, which were named as alloys S1, S2, and S3. The single crystal bars with 7 mm in diameter and 80 mm in length were produced by a seeding technique in a directional

Contributing Editor: Jürgen Eckert

<sup>a)</sup>Address all correspondence to this author.

e-mail: zhjscott@nwpu.edu.cn

DOI: 10.1557/jmr.2016.98

solidification vacuum furnace with 250 °C/cm thermal gradient and 100 μm/s withdrawal rate. Finally, their compositions were analyzed by atomic absorption spectrophotometry, and the initial chemical compositions are listed in Table I.

Three alloys were subjected to three different solution treatments as presented in Table II. Then, an aging heat treatment was performed at: 1170 °C/4 h air cooling (AC) → 870 °C/24 h AC. After solution and aging treatment, the thermal exposure was performed at 1000 °C for 100, 200, 500, and 1000 h.

The samples were cut perpendicularly to [001] growth direction and etched in a solution of 1HNO<sub>3</sub>:2HF:4C<sub>3</sub>H<sub>8</sub>O<sub>3</sub>. The NETZSCH-STA409CD differential scanning calorimetry (DSC; Netzsch-Gerätebau GmbH, Selb, Germany) was used to determine the liquidus ( $T_l$ ), solidus ( $T_s$ ), and  $\gamma'$  solvus ( $T_{\gamma'}$ ) temperature. The JEOL JAX-8100 electron probe micro-analysis (EPMA; JEOL Ltd., Tokyo, Japan) was used to analysis the compositions of the dendrite core and interdendritic region, and the compositions of  $\gamma$  and  $\gamma'$  phase, at least five measurement points were selected on each zone. The Tecnai F<sub>30</sub> G<sup>2</sup> transmission electron microscope (TEM; FEI Company, Eindhoven, The Netherlands) with energy dispersive spectrometer (EDS) was used to identify the TCP phase. The ZEISS SUPRA 55 field emission scanning electron microscope (SEM; Carl Zeiss, Oberkochen, Germany) was used to characterize the microstructure of these alloys. Furthermore, the mean size and volume fraction of  $\gamma'$  phase were measured by a quantitative metallography using at least 300 particles for each one thermal exposure period. The size of  $\gamma'$  phase and the thermal exposure time could be fitted by using Lifshitz–Slyozov–Wagner LSW formula as below:

$$\bar{r}^3 - \bar{r}_0^3 = Kt \quad , \quad (1)$$

TABLE I. Initial chemical compositions of three investigated alloys (wt%).

Alloy	Al	Ta	Mo	W	Re	Cr	Co	Ni
S1	5.8	8.0	1.0	6.0	5.0	2.4	4.0	Bal.
S2	5.7	7.9	1.0	6.1	5.1	2.4	8.5	Bal.
S3	5.7	8.0	1.0	6.0	5.0	2.5	11.5	Bal.

Bal. = Balance

TABLE II. Solution heat treatment schedules of the three alloys.

Alloy	Solution heat treatment
S1	1310 °C/1 h → 1315 °C/2 h → 1323 °C/2 h → 1328 °C/2 h → 1333 °C/3 h → 1338 °C/12 h → 1343 °C/24 h AC
S2	1304 °C/1 h → 1309 °C/2 h → 1317 °C/2 h → 1322 °C/2 h → 1327 °C/3 h → 1332 °C/12 h → 1337 °C/24 h AC
S3	1300 °C/1 h → 1305 °C/2 h → 1313 °C/2 h → 1318 °C/2 h → 1323 °C/3 h → 1328 °C/12 h → 1333 °C/24 h AC

where  $\bar{r}_0$  was the initial particle radius,  $\bar{r}$  was the instantaneous particle radius,  $K$  was the rate constant, and  $t$  was the coarsening time. Obviously,  $\bar{r} = a/2$  and  $\bar{r}_0 = a_0/2$ . To characterize the coarsening mechanism of  $\gamma'$  phase, the plots of  $(a/2)^3 - (a_0/2)^3$  versus  $t$  was also constructed.

### III. RESULTS

#### A. Microstructure and segregation of as-cast alloys

Although three experimental superalloys have different compositions, their microstructures at as-cast are basically similar because they have been produced with the same thermal gradient and withdrawal rate. Therefore, a typical microstructure at as-cast is shown in Fig. 1(a), which is composed of some regularly arranged dendrites and interdendritic eutectics. Further, the segregation ratios of alloying elements are investigated, which can be defined as:

$$k^i = C_{DC}^i / C_{ID}^i \quad , \quad (2)$$

where  $C_{DC}$  and  $C_{ID}$  are contents of alloying elements in dendrite core and interdendritic region, respectively. The results are listed in Fig. 2. It is clear that: (i)  $k^{Re} > k^W > 1$ , showing that Re and W segregate to the dendrite core and the segregation of Re is more severe than that of W; (ii)  $k^{Ta} < k^{Al} < 1$ , indicating that Ta and Al segregate to the interdendritic region and the segregation of Ta is more severe than that of Al; (iii) with the increase of Co content, the segregation of Re, W, and Ta increase slightly, which indicates that the segregation degree of alloying elements is aggravated.

#### B. Microstructure and segregation after solution heat treatment

The microstructure after solution treatment is shown in Fig. 1(b). It is seen that the interdendritic eutectics have been basically eliminated, and the dendritic morphology is invisible. Furthermore, the segregation ratios of alloying elements after solution treatment are shown in Fig. 2, where segregation ratios of the elements are decreased obviously. It is very interesting that these segregation ratios are basically close to 1, showing a very good solution treatment result.

#### C. Microstructure after aging treatment

The typical microstructures of three alloys after aging treatment are shown in Fig. 3. It can be seen that there are only  $\gamma$  and  $\gamma'$  phase in microstructure without any other phase, and the  $\gamma'$  phase in alloy S1 presents the best typical cuboidal morphology. Furthermore, the volume fractions of  $\gamma'$  phase in three alloys are measured to be about 75%, which indicates that the Co addition has little

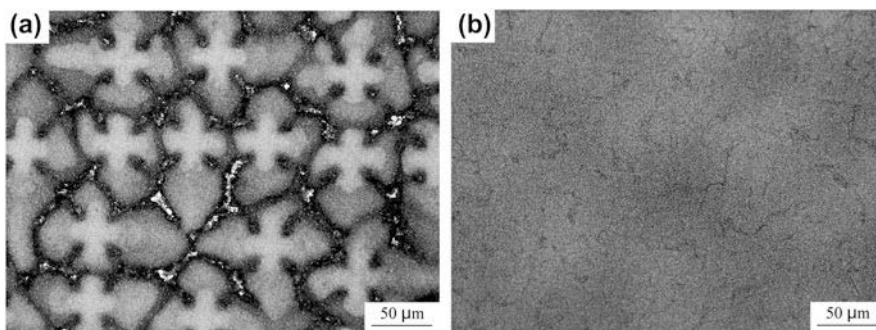
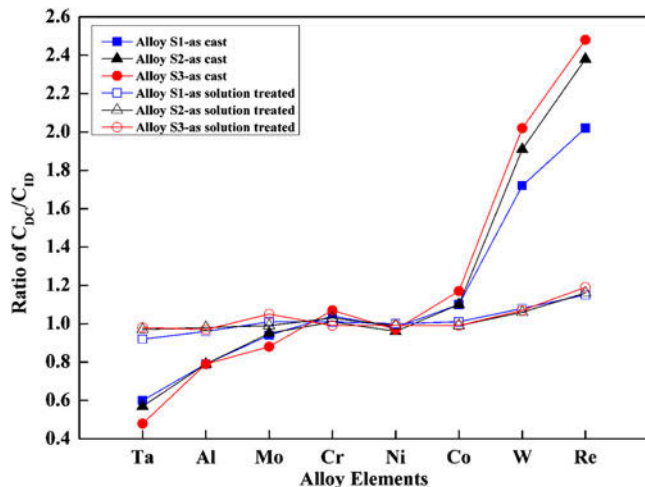


FIG. 1. Microstructure of alloy S1 as-cast (a), and with solution treatment (b).

FIG. 2. Segregation ratio  $k$  of alloying elements with and without solution treatment.

effect on the  $\gamma'$  volume fraction. However, the average size of  $\gamma'$  phase decreases gradually from 476 to 421 nm with the increase of Co content.

#### D. Coarsening of $\gamma'$ phase during the thermal exposure

Morphology evolution of  $\gamma'$  phases during thermal exposure at 1000 °C is shown in Fig. 4. It is seen that the cuboidal  $\gamma'$  phases begin to present some round corners at the thermal exposure for 500 h; after 1000 h,  $\gamma'$  phases begin to coalesce and present rectangle morphology in alloys S1 and S2. However, the morphology of  $\gamma'$  phases is maintaining a good cuboidal morphology in alloy S3 although the thermal exposure time has reached to 1000 h.

Furthermore, the size of  $\gamma'$  phase at different thermal exposure times is measured as shown in Fig. 5. It can be seen that the size of  $\gamma'$  phase in alloy S1 is the largest but the smallest in alloy S3 after the thermal exposure for 1000 h. After a linear fitting, it can be seen that the coarsening of  $\gamma'$  phase complies with the LSW theory.<sup>22–26</sup> And the coarsening rate constants of  $\gamma'$  phase are about  $7.29 \times 10^{-5}$ ,  $4.48 \times 10^{-5}$ , and  $1.87 \times 10^{-5}$  for alloys S1, S2, and S3, respectively, which indicates that the coarsening rate constant of  $\gamma'$  phase can be decreased with increasing

Co content. Therefore, the stability of  $\gamma'$  phases can be improved by Co content addition.

#### E. The precipitation of TCP phase during thermal exposure

The precipitation of TCP phase during thermal exposure process is also a very important factor in effecting the mechanical property. Therefore, morphology of TCP phase in alloy S1 and alloy S2 after the thermal exposure at 1000 °C for different times are shown in Figs. 6(a)–6(h). In alloy S1, a few acicular TCP phases begin to form with 2.07% volume fraction after thermal exposure for 100 h. And then, their volume fraction increases continuously from 4.28% at 200 h to 12.17% at 1000 h, showing an obvious precipitation and coarsening phenomenon. However, there is no basically TCP phase precipitation at only 100 h in alloy S2. Prolonging this exposure time to 200 h, a few blocky TCP phases begin to form with only 0.35% volume fraction. At 500 h, a few fine acicular TCP phase can be found and their volume fraction increases to 1.21%. At 1000 h, these TCP phases grow up with 5.1% volume fraction. Compared with the microstructures in alloys S1 and S2, it is interesting that no TCP phase can be formed in alloy S3 as shown in Figs. 6(i)–6(l).

Furthermore, the relation between the volume fraction of TCP phases and the thermal exposure time is shown in Fig. 7. It can be seen that the precipitation rate in alloy S1 is much larger than that in alloys S2 within 200 h. After 200 h, it decreases slowly and then increases rapidly after 500 h. And, the volume fraction of TCP phases in alloy S2 is less than that in alloy S1, which indicates that Co is beneficial to postpone and suppress the formation of TCP phases.

Figure 8 further shows the morphology and corresponding selected area diffraction patterns (SADP) of TCP phases after thermal exposure for 100 h in alloy S1 and for 200 h in alloy S2. It can be seen that some acicular TCP phases present the mutually perpendicular distribution in Fig. 8(a), and some blocky TCP phases distributes randomly in  $\gamma$  matrix in Fig. 8(b). Although they present two different morphologies, the results from SADP show that both of them are actually  $\sigma$  phase with

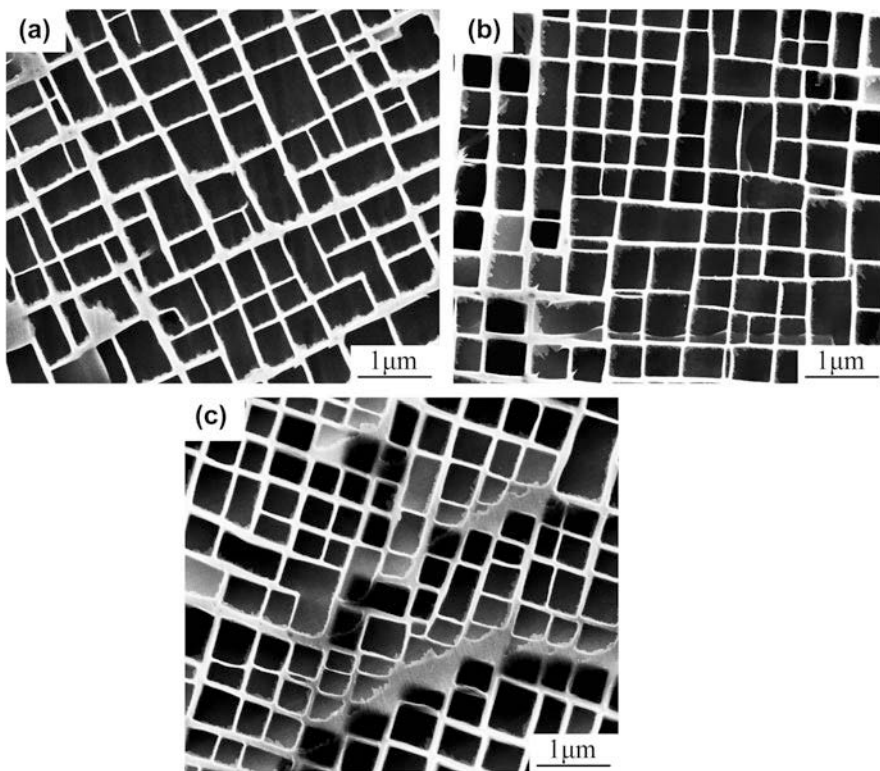


FIG. 3. Typical microstructure of alloy S1 (a), alloy S2 (b), and alloy S3 (c) after aging treatment.

$a = b = 0.912$  nm,  $c = 0.472$  nm lattice parameter. Furthermore, EDS analysis in Figs. 8(e) and 8(f) shows that two TCP phases basically have the same composition with mainly Re, W, and Mo enrichments.

#### IV. DISCUSSION

Two important aspects should be taken into consideration in discussing the microstructural stability of Ni-based single crystal superalloys during the thermal exposure: (i) stability of  $\gamma'$  phase; (ii) TCP phase precipitation. The stability of  $\gamma'$  phase is generally controlled by the elements diffusion and the interface reaction, and the precipitation of TCP phase is controlled by the local supersaturation in  $\gamma$  matrix, which is influenced by the partitioning ratio of  $\gamma/\gamma'$  phase. Partitioning ratio of  $\gamma/\gamma'$  phase is controlled by elements distribution in both  $\gamma$  and  $\gamma'$  phase. It not only affects the misfit and the morphology of  $\gamma'$  phase, but also determines the content of alloying elements in  $\gamma$  matrix. Chen et al. believed that if the content of alloying elements exceeded the solid solubility limitation in  $\gamma$  matrix, it would form TCP phases.<sup>27</sup> In the following sections, these discussions will be presented in detail.

##### A. Effect of Co on the segregation

In the directional solidification process of single crystal superalloy, different alloying elements have different

segregations. For example, Re and W elements mainly enrich in the dendrite core while Ta and Al elements enrich in interdendritic region. In the last stage of solidification, the forming elements of  $\gamma'$  phase such as Ta and Al further enrich in the interdendritic zone to form the  $\gamma/\gamma'$  eutectic. Elements segregation and eutectics quantity are two important factors in controlling the mechanical property, especially for the high-temperature creep property. Therefore, the solution treatment is needed to eliminate the eutectics and homogenize the alloying elements.

The larger solidification temperature range leads to the more severe element segregation.<sup>28</sup> The solidification temperature range determined by DSC in three alloys are 50, 54, and 57 °C, respectively, which means that the Co content addition can enlarge solidification temperature range, therefore results in the aggravation of the elements segregation.

Figure 2 shows that segregations of Al, Ta, W, and Re are decreased obviously after solution treatment, especially the segregation of Re is also reduced significantly. It is because that the dendrite size of the experimental alloy is very small, the primary dendrite arm spacing is only 90  $\mu\text{m}$ . Simultaneously, the time of solution treatment is very long so that the alloying elements have enough time to diffuse. Therefore, the segregation ratios of refractory elements are decreased significantly to achieve a good homogenizing effect after solution treatment.

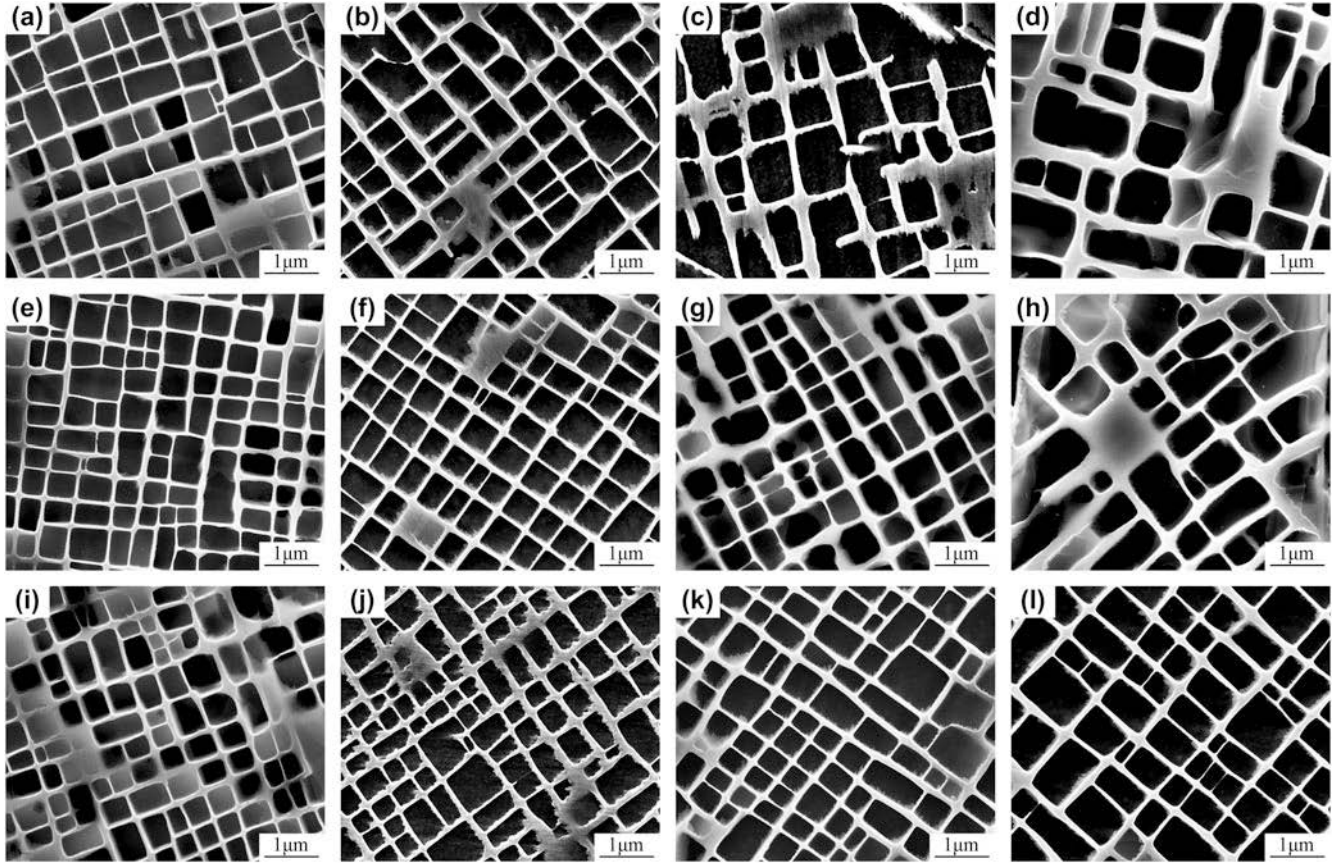


FIG. 4. Morphology of  $\gamma'$  phase in three alloys during thermal exposure at 1000 °C: [(a)–(d)] for alloy S1, [(e)–(h)] for alloy S2, and [(i)–(l)] for alloy S3 at 100, 200, 500, and 1000 h, respectively.

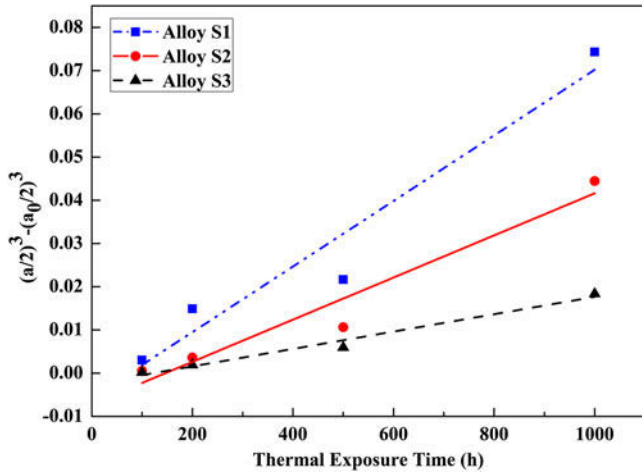


FIG. 5. Plot of third power of  $\gamma'$  size as a function of thermal exposure time at 1000 °C for three alloys.

## B. Effect of Co on morphology of $\gamma'$ phase

Morphology and stability of  $\gamma'$  phase are closely related to the misfit between  $\gamma$  phase and  $\gamma'$  phase.<sup>29,30</sup> The misfit can be calculated as:

$$\delta = 2(a_{\gamma'} - a_{\gamma}) / (a_{\gamma'} + a_{\gamma}) , \quad (3)$$

where  $a_{\gamma'}$  and  $a_{\gamma}$  are lattice constant of  $\gamma'$  phase and  $\gamma$  phase, respectively. Morphology of  $\gamma'$  phase is determined by  $\delta$ . When  $\delta$  value is close to 0, the morphology of  $\gamma'$  phase is basically spherical shape, in turn, when  $\delta$  value is far away from 0, its morphology will be changed to the cuboidal shape. The compositions of  $\gamma'$  phase and  $\gamma$  phase determine the partitioning ratio of alloying elements and further influence the  $\delta$  value, which results in a different morphology of  $\gamma'$  phase.

The elemental partitioning ratio of  $\gamma/\gamma'$  phase after aging treatment determined by EPMA is shown in Table III. It can be seen that W, Mo, Cr, and Re elements enrich in  $\gamma$  matrix while Al and Ta elements enrich in  $\gamma'$  phase, and Re element has the highest partitioning ratio. With the increase of Co content, the enrichment of Al in  $\gamma'$  phase and that of W, Mo, Cr, and Re in  $\gamma$  matrix are reduced gradually. For example, the partitioning ratio of Re is reduced from 6.3 to 3.1.

In alloy S1, W, Mo, Cr, and Re elements enrich in  $\gamma$  matrix (especially Re), which can enlarge the lattice parameter  $a_{\gamma}$ . Therefore, the absolute value of  $a_{\gamma'} - a_{\gamma}$  will be increased, and the value of  $\delta$  also becomes more negative. When Co content increases to 8.5%, the enrichment of W, Mo, Cr, and Re in  $\gamma$  matrix is reduced so that the lattice parameter  $a_{\gamma}$  reduces while the lattice

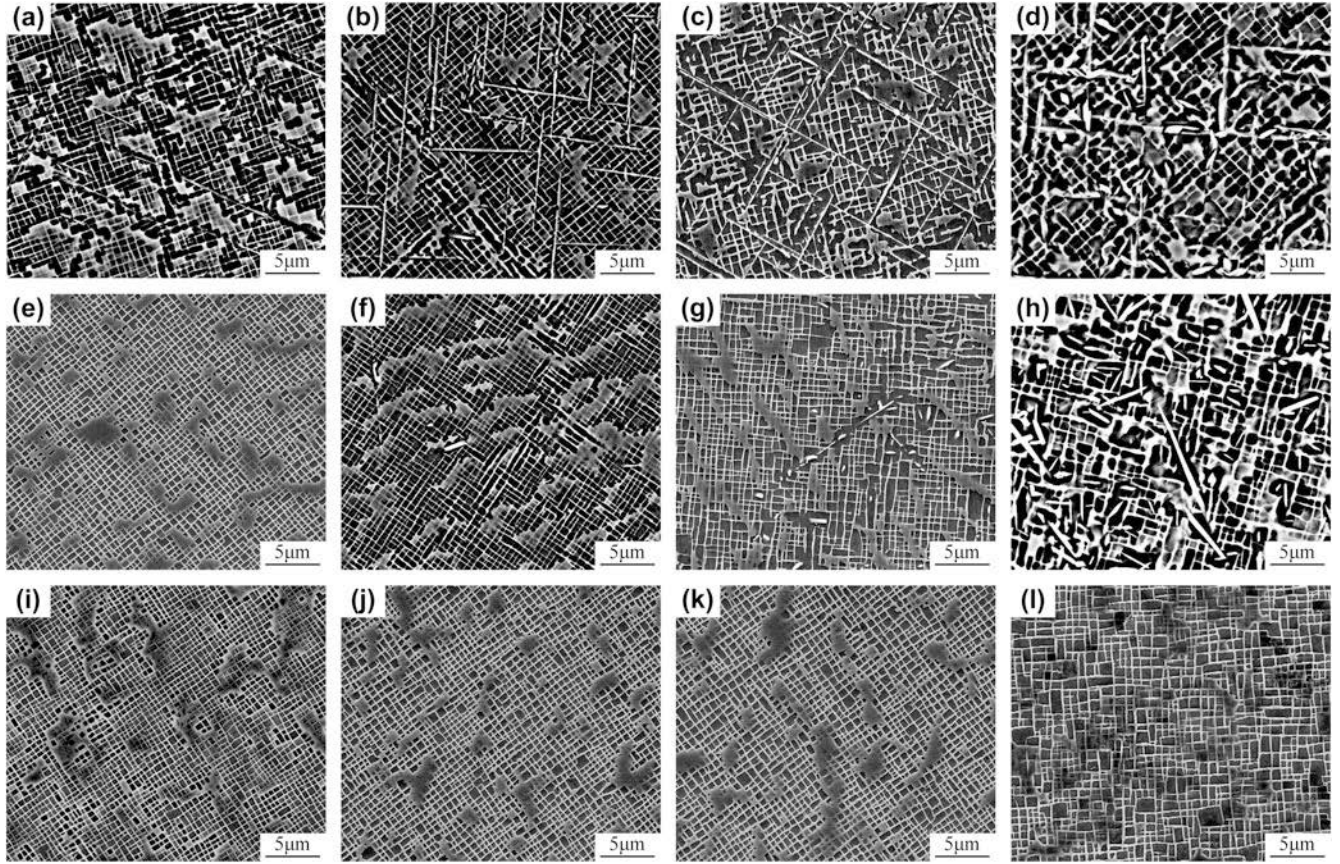


FIG. 6. Morphology of TCP phase in three alloys during thermal exposure at 1000 °C: [(a)–(d)] for alloy S1, [(e)–(h)] for alloy S2, and [(i)–(l)] for alloy S3 at 100, 200, 500, and 1000 h, respectively.

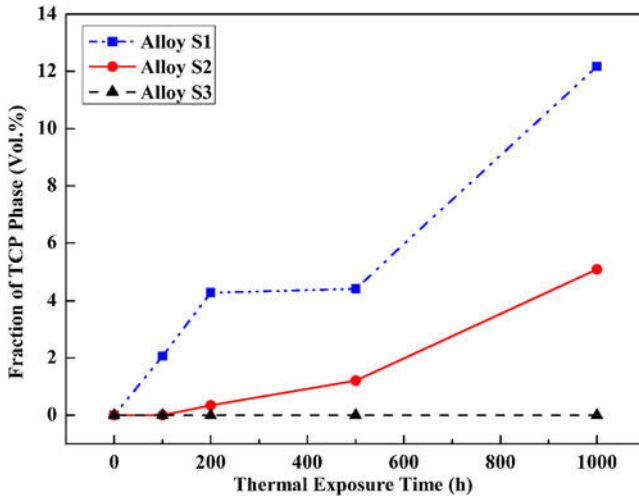


FIG. 7. Plot of TCP phase volume fraction with thermal exposure time at 1000 °C for three alloys.

parameter  $a_{\gamma'}$  increases, and the absolute value of  $\delta$  will be reduced. With increasing Co content to 11.5%, only the enrichment of Re is reduced, but the enrichment of other elements are not changed obviously comparing with that in alloy S2. Therefore, the absolute value of  $\delta$  is

reduced slightly. Finally, the  $\gamma'$  phase in alloy S1 presents the best cuboidal shape whereas the  $\gamma'$  phase in alloy S3 has the worst cuboidal shape, as shown in Fig. 3. In addition, based on the calculated result by thermodynamic software JMatPro, the misfit of  $\gamma/\gamma'$  phases is changed from negative value to zero with the increase of Co content as shown in Table III, and the trend is consistent with the discussion above.

### C. Effect of Co on coarsening of $\gamma'$ phase

The coarsening of  $\gamma'$  phase complies with LSW theory as shown in Fig. 5, the slope  $K$  is coarsening rate constant, which is defined as:

$$K = 2vDC_e V_m^2 / \rho_c^2 RT , \quad (4)$$

where  $v$  is the interfacial free energy of the particle/matrix interface,  $D$  is the diffusion coefficient of solutes in matrix,  $C_e$  is the concentration of solute (forming elements of  $\gamma'$  phase) in equilibrium with a particle of infinite radius,  $V_m$  is the molar volume of precipitates,  $\rho_c$  is the numerical constant dependent on the distribution of particle sizes ( $\rho_c = 3/2$  according to LSW theory),  $R$  is the gas constant, and  $T$  is the absolute temperature.

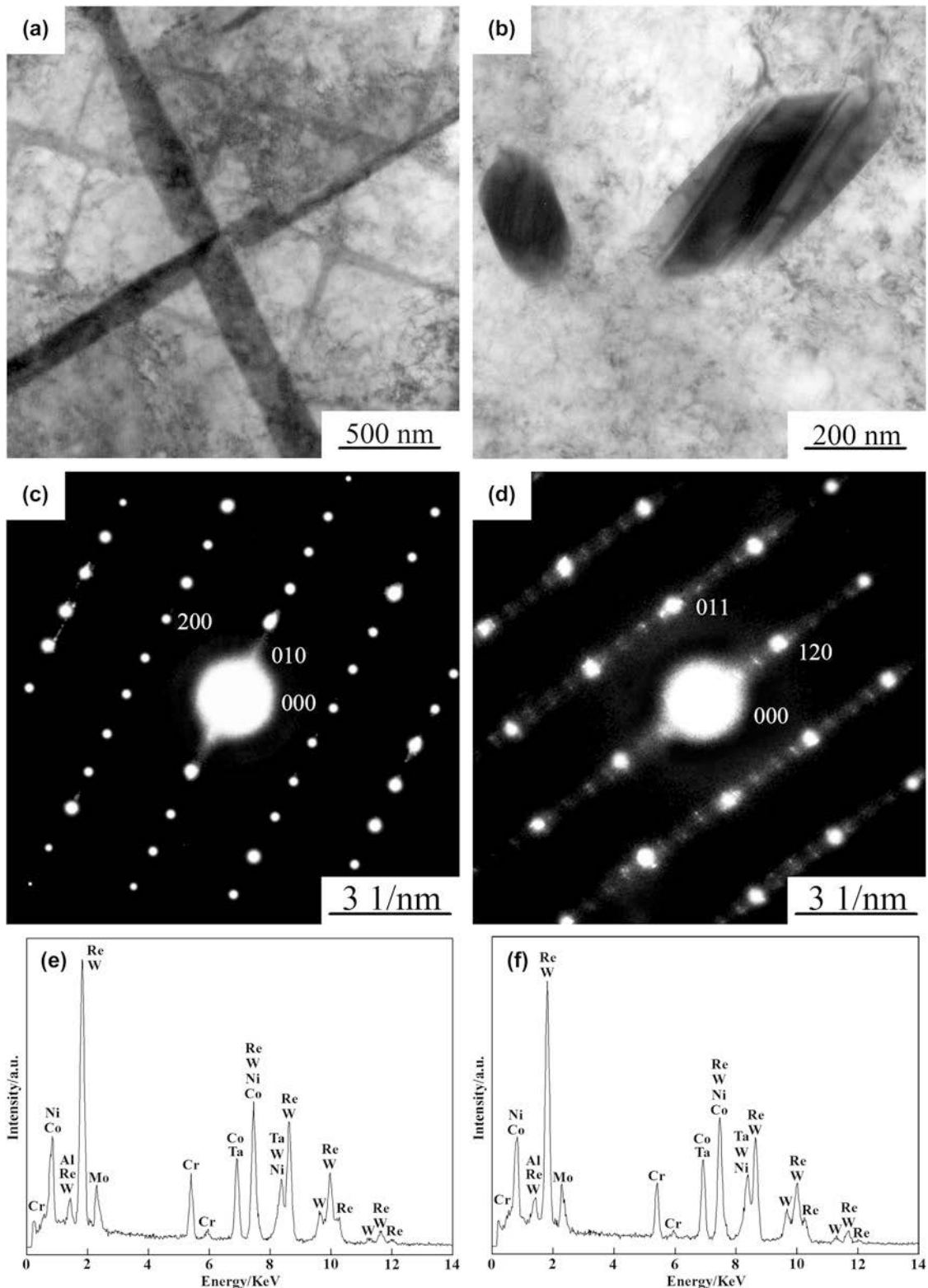


FIG. 8. TEM micrograph [(a) and (b)] and the corresponding SADP [(c) and (d)] with EDS analysis [(e) and (f)] of TCP phases precipitate after thermal exposure 100 h for alloy S1 and 200 h for alloy S2, respectively.

According to the Eq. (4),  $\rho_c$ ,  $R$ , and  $T$  are constants at same temperature. The only difference among three alloys is the Co content. The increase of Co content

has basically no influence on the  $V_m$  as shown in Fig. 3. And, the interface free energy  $v$  consists of two parts: one is related to the structure of  $\gamma/\gamma'$  interface; the other is

TABLE III. Elemental partitioning ratio of three alloys after aging treatment and the lattice misfit  $\delta$  determined by JMatPro.

Alloy	Al	Ta	Ni	Co	Cr	Mo	W	Re	$\delta$ (1000 °C)
S1	0.59	0.56	0.90	1.51	2.71	2.94	1.56	6.33	$-5.42 \times 10^{-4}$
S2	0.69	0.61	0.91	1.44	2.30	2.21	1.36	3.35	$-2.64 \times 10^{-4}$
S3	0.75	0.58	0.92	1.37	2.01	2.14	1.37	3.12	$-1.13 \times 10^{-4}$

related to the chemistry of interface, both of them rarely vary with the increase of Co content. Therefore, the  $v$  is also constant for three alloys at same temperature. Accordingly, this Eq. (4) will be defined as:

$$D = AK/C_e , \quad (5)$$

where  $A = \rho_c^2 RT/2vV_m^2$ . And now, a formula can be obtained as follows:

$$D_1/D_2 = (K_1/K_2)(C_{e2}/C_{e1}) , \quad (6)$$

It can be seen that the concentration of Al as the forming element of  $\gamma'$  phase increases in matrix with the increase of Co content from Table III, so there is  $C_{e1} < C_{e2} < C_{e3}$  for alloys S1, S2, and S3. Based on the results in Fig. 5, it can be obtained that  $K_1 > K_2 > K_3$ , and further resulting  $D_1 > D_2 > D_3$ . It indicates that the diffusion coefficient is decreased with the increase of Co content at the same temperature. In other words, Co element may restrain the diffusion.

#### D. Effect of Co on size of $\gamma'$ phase

For  $\gamma'$  phase, the higher solvus temperature results in the earlier precipitation during cooling process after the solution treatment. In other words, it provides a longer time to grow for  $\gamma'$  phase, and the size of  $\gamma'$  phase before aging treatment will become larger.<sup>19,20</sup> Solvus temperatures of  $\gamma'$  phase have been determined by DSC as 1288, 1276, and 1271 °C, respectively, which indicates that the solvus temperatures are decreased gradually with the increase of Co content. Therefore, the grow time for  $\gamma'$  phase in alloy S1 is the longest but the shortest in alloy S3. Besides, the above section indicates that the elements diffusion can be restrained with the increase of Co content, therefore, the growth rate of  $\gamma'$  is also decreased during aging treatment, and the size of  $\gamma'$  in alloy S1 is the largest but the smallest in alloy S3.

#### E. Effect of Co on precipitation of TCP phase

Because the segregation of alloying elements in three alloys is basically same after different solution treatments in discussing the precipitation process of TCP phase, it is only needed to consider the partitioning ratio of  $\gamma/\gamma'$  phase. Solid solubility limitation of Ni matrix at 870 °C can be calculated by the formula proposed by Chen<sup>27</sup>:

$$S_{T=870\text{ }^\circ\text{C}} = 44.78448 - 68.5517\Delta R - 3.4853\Delta N^2 - 31.9337\Delta E^{1/3} , \quad (7)$$

where  $\Delta R$  and  $\Delta N$  are the differences of atomic radius and electronegativity between solute element and Ni element, respectively, and  $\Delta E^{1/3}$  is the difference of cubic root of electron number in outer shell between solute element and Ni element. Then to calculate  $\Delta S$  by using Eq. (8):

$$\Delta S = S_{T=870\text{ }^\circ\text{C}} - S_g , \quad (8)$$

where  $S_g$  is the total actual content of alloying elements in  $\gamma$  matrix. It illustrates that when  $\Delta S < 0$ , TCP phase will be precipitated, and when  $\Delta S > 0$ , no TCP phase can be found.

According to the above calculation method, the precipitation of TCP phase is influenced by two factors: (i)  $S_{T=870\text{ }^\circ\text{C}}$ -solid solubility limitation of  $\gamma$  matrix; (ii)  $S_g$ -actual content of alloying elements in  $\gamma$  matrix. Chen et al.<sup>27</sup> believed that the increase of low solid solubility alloying elements, such as Al, Ta, Nb, and Hf reduced the solid solubility limitation, whereas the increase of Co, Ru content as high solid solubility alloying elements increased the solid solubility limitation of  $\gamma$  matrix. Therefore, it can be concluded  $S_{4\text{Co}\%} < S_{8.5\text{Co}\%} < S_{11.5\text{Co}\%}$  for three investigated alloys.

Table III illustrates that the increase of Co content reduces the partitioning ratio of Mo, Cr, Ta, W, and Re, which means the enrichment of such elements decreases in  $\gamma$  matrix. Therefore, the total actual content of alloying elements should be decreased as:  $S_{g4\text{Co}\%} > S_{g8.5\text{Co}\%} > S_{g11.5\text{Co}\%}$ , further resulting in  $\Delta S_{4\text{Co}\%} < \Delta S_{8.5\text{Co}\%} < \Delta S_{11.5\text{Co}\%}$ . The calculated results of  $\Delta S$  of three experiment alloys are -1.82, -1.07, and 0.82, respectively. It is clear that the Co content is proportional to numerical value of  $\Delta S$ , which means the trend of TCP phase precipitation is decreased. As seen from Figs. 6 and 7, when Co content increases from 4 to 8.5%, the precipitation time of TCP phase is increased and the volume fraction is decreased until no TCP phase can be formed in 11.5% Co content alloy. It is corresponding to the experiment results, which indicates that the increase of Co content is able to postpone and restrain the precipitation of TCP phase.

#### F. Effect of Co on morphology of TCP phase

Figure 8 shows that  $\sigma$  phase has acicular and blocky-shaped morphology with the basically same compositions. This phenomenon was also found in other TCP phases by other researchers where they believed that the morphology difference was caused by the different W/Mo ratio.<sup>31,32</sup> A high W/Mo ratio led to TCP phase with an acicular shape and a low W/Mo ratio resulted in TCP phase with a blocky shape. Table IV shows Re, W,

TABLE IV. Re, W, and Mo content of acicular  $\sigma$  phase in alloy S1 and blocky  $\sigma$  phase in alloy S2 (at.%).

Phase	Re	W	Mo	W/Mo	Re/Mo
Acicular $\sigma$	23.46	12.59	8.32	1.51	2.82
Blocky $\sigma$	21.92	13.68	10.34	1.32	2.12

and Mo contents of acicular  $\sigma$  phase in alloy S1 after the thermal exposure for 100 h and blocky  $\sigma$  phase in alloy S2 after thermal exposure for 200 h. It can be found that the ratio of W/Mo in acicular  $\sigma$  phase is higher than that in blocky  $\sigma$  phase. In addition, three investigated alloys contain 5% Re, which significantly accelerates the precipitation of TCP phase. Moreover, because the content of Re in TCP phase is very high, the ratio of Re/Mo in two  $\sigma$  phases is also analyzed. It can be found that the ratio of Re/Mo in acicular  $\sigma$  phase is higher than that in blocky  $\sigma$  phase, and the ratio of Re/Mo is higher than that of W/Mo, which means the acicular  $\sigma$  phase has relatively higher Re and W contents and lower Mo content. And, the partitioning ratios of  $\gamma/\gamma'$  phases in three alloys in Table III shows that the contents of W and Re in  $\gamma$  matrix in alloy S1 is higher than that of alloy S2, which may be a reason that the acicular  $\sigma$  phase is formed first in alloy S1 and the blocky  $\sigma$  phase is precipitated first in alloy S2.

## V. CONCLUSION

(1) The alloying elements segregation was slightly aggravated in as-cast alloys with the increase of Co content, and it was significantly decreased after solution treatment. The enrichments of Re, Mo, and Cr in  $\gamma$  matrix were decreased obviously with the increase of Co content.

(2) The increase of Co content could decrease the cuboidal degree and the size of  $\gamma'$  phase, and restrain the growth and deformation of  $\gamma'$  phase during thermal exposure.

(3) TCP phase formed during thermal exposure was identified as  $\sigma$  phase in 4% Co and 8.5% Co alloy. However, no TCP phase was found in 11.5% Co alloy. Therefore, the increase of Co content may change the morphology and impede the precipitation of TCP phase.

## ACKNOWLEDGMENTS

This work was supported by the National High Technology Research and Development Program of China (2012AA03A511), the State Key Program of National Natural Science of China (51331005), the Natural Science Foundation of Shaanxi Province (2014JM622), the NWPU Foundation for Basic Research (3102014JCQ01022), and the Advanced Aeroengine Collaborative Innovation Center of China.

## REFERENCES

- Z. Hu, L. Liu, T. Jin, and X. Sun: Development of the Ni-base single crystal superalloys. *Aeroengine* **3**, 1 (2005).
- J. Guo: The current situation of application and development of superalloys in the fields of energy industry. *Acta Metall. Sin.* **5**, 513 (2010).
- R.C. Reed, T. Tao, and N. Warnken: Alloys-by-design: Application to nickel-based single crystal superalloys. *Acta Mater.* **57**, 5898 (2009).
- S. Walston, A. Cetel, R. Mackay, K. O'Hara, D. Duhl, and R. Dreshfield: Joint development of a fourth generation single crystal superalloy. In *Superalloys 2004*, K.A. Green, T.M. Pollock, H. Harada, T.E. Howson, R.C. Reed, J.J. Schirra, and S. Walston, eds. (TMS: Warrendale, 2004); p. 1.
- P. Caron: High  $\gamma'$  solvus new generation nickel-based superalloys for single crystal turbine blade applications. In *Superalloys 2000*, T.M. Pollock, R.D. Kissinger, R.R. Bowman, K.A. Green, M. McLean, S. Oison, and J.J. Schirra, eds. (TMS: Warrendale, 2000); p. 737.
- A. Sato, H. Harada, A.C. Yen, K. Kawagishi, T. Kobayashi, Y. Koizumi, T. Yokokawa, and J.X. Zhang: A 5th generation sc superalloy with balanced high temperature properties and processability. In *Superalloys 2008*, R.C. Reed, K.A. Green, P. Caron, T.P. Gabb, M.G. Fahrmann, E.S. Huron, and S.A. Woodard, eds. (TMS: Warrendale, 2008); p. 131.
- A. Sato, A.C. Yeh, T. Kobayashi, T. Yokokawa, H. Harada, T. Murakumo, and J.X. Zhang: Fifth generation Ni based single crystal superalloy with superior elevated temperature properties. *Energy Mater.* **1**, 19 (2007).
- G.E. Fuchs: Solution heat treatment response of a third generation single crystal Ni-base superalloy. *Mater. Sci. Eng., A* **300**, 52 (2001).
- C.M.F. Rae and R.C. Reed: The precipitation of topologically close-packed phases in rhenium-containing superalloys. *Acta Mater.* **49**, 4113 (2001).
- R. Rettig and R.F. Singer: Numerical modelling of precipitation of topologically close-packed phases in nickel-base superalloys. *Acta Mater.* **59**, 317 (2011).
- O. Lavigne, C. Ramusat, S. Drawin, P. Caron, D. Boivin, and J.L. Pouchou: Relationships between microstructural instabilities and mechanical behaviour in new generation nickel-based single crystal superalloys. In *Superalloys 2004*, K.A. Green, T.M. Pollock, H. Harada, T.E. Howson, R.C. Reed, J.J. Schirra, and S. Walston, eds. (TMS: Warrendale, 2004); p. 667.
- W.S. Walston, K.S. O'Hara, E.W. Ross, T.M. Pollock, and W.H. Murphy: René N6: third generation single crystal superalloy. In *Superalloys 1996*, R.D. Kissinger, D.J. Deye, D.L. Anton, A.D. Cetel, M.V. Nathal, T.M. Pollock, and D.A. Woodford, eds. (TMS: Warrendale, 1996); p. 27.
- M.V. Acharya and G.E. Fuchs: The effect of long-term thermal exposures on the microstructure and properties of CMSX-10 single crystal Ni-base superalloys. *Mater. Sci. Eng., A* **381**, 143 (2004).
- X. Tan, J. Liu, T. Jin, Z. Hu, H.U. Hong, B.G. Choi, I.S. Kim, Y.S. Yoo, and C.Y. Jo: Effect of ruthenium on precipitation behavior of the topologically close-packed phase in a single-crystal Ni-based superalloy during high-temperature exposure. *Metall. Mater. Trans. A* **43**, 3608 (2012).
- M.S.A. Karunaratne, C.M.F. Rae, and R.C. Reed: On the microstructural instability of an experimental nickel-based single-crystal superalloy. *Metall. Mater. Trans. A* **32**, 2409 (2001).
- W. Wang, T. Jin, J. Liu, X. Sun, H. Guan, and Z. Hu: Role of Re and Co on microstructures and  $\gamma'$  coarsening in single crystal superalloys. *Mater. Sci. Eng., A* **479**, 148 (2008).

17. G.L. Erickson: The development of the CMSX-1IB and CMSX-1IC alloys for industrial gas turbine application. In *Superalloys 1996*, R.D. Kissinger, D.J. Deye, D.L. Anton, A.D. Cetel, M.V. Nathal, T.M. Pollock, and D.A. Woodford, eds. (TMS: Warrendale, 1996); p. 45.
18. G.L. Erickson: The development and application of CMSX-10. In *Superalloys 1996*, TMS: Warrendale, 1996); p. 35.
19. M.V. Nathal, R.D. Maier, and L.J. Ebert: The influence of cobalt on the microstructure of the nickel-base superalloy MAR-M247. *Metall. Trans. A* **13**, 1775 (1982).
20. M.V. Nathal and L.J. Ebert: The influence of cobalt, tantalum, and tungsten on the microstructure of single crystal nickel-base superalloys. *Metall. Trans. A* **16**, 1849 (1985).
21. M.V. Nathal and L.J. Ebert: The influence of cobalt, tantalum, and tungsten on the elevated temperature mechanical properties of single crystal nickel-base superalloys. *Metall. Trans. A* **16**, 1863 (1985).
22. I.M. Lifshitz and V.V. Slyozov: The kinetics of precipitation from supersaturated solid solutions. *J. Phys. Chem. Solids* **1–2**, 35 (1961).
23. C. Wagner: Theorie der alterung von niederschlägen durch umlösen. *Z. Elektrochem.* **7–8**, 581 (1961).
24. E.H. Vandermolen, J.M. Oblak, and O.H. Krieger: Control of  $\gamma'$  particle size and volume fraction in the high temperature superalloy Udimet 700. *Metall. Trans.* **2**, 1627 (1971).
25. A.F. Giamei and D.L. Aanton: Rhodium additions to a Ni-base superalloy: Effects on microstructure. *Metall. Trans.* **16**, 1997 (1985).
26. W. Sun: Kinetics for coarsening co-controlled by diffusion and a reversible interface reaction. *Acta Mater.* **55**, 313 (2007).
27. Z. Chen, Y. Han, Z. Zhong, P. Wei, and M. Yan: New phase stability prediction method of nickel base single crystal superalloys. *J. Aeronaut. Mater.* **4**, 13 (1998).
28. S. Jiao, J. Zhang, T. Jin, C. Wang, H. Wang, L. Liu, and H. Fu: DTA research of a third generation Ni-based single crystal superalloy. *Rare Met. Mater. Eng.* **5**, 1028 (2013).
29. M. Fährmann, P. Fratzl, O. Paris, E. Fährmann, and W.C. Johnson: Influence of coherency stress on microstructural evolution in model Ni-Al-Mo alloys. *Acta Metall. Mater.* **3**, 1007 (1995).
30. T. Wang, G. Sheng, Z. Liu, and L. Chen: Coarsening kinetics of  $\gamma'$  precipitates in the Ni-Al-Mo system. *Acta Mater.* **56**, 5544 (2008).
31. X. Qin, J. Guo, C. Yuan, G. Yang, L. Zhou, and H. Ye:  $\mu$ -Phase behavior in a cast Ni-base superalloy. *J. Mater. Sci.* **44**, 4840 (2009).
32. T. Wen, J. Li, L. Liu, L. Chen, and T. Jin: Effect of long-term aging on microstructure evolution and stress rupture properties of Ni-based single crystal superalloy. *Rare Met. Mater. Eng.* **2**, 230 (2012).